Title:

Genome editing of *Capsaspora owczarzaki* suggests an ancestral function of the Hippo signaling effector YAP/TAZ/Yorkie in cytoskeletal dynamics but not proliferation

Authors:

Jonathan E Phillips[1], Maribel Santos[1], Mohammed Kanchwala[2], Chao Xing[2], Duojia Pan[1*]

Affiliations:

[1]Department of Physiology, Howard Hughes Medical Institute, University of Texas Southwestern Medical Center, Dallas, Texas 75390, USA

[2]Eugene McDermott Center for Human Growth & Development, Departments of Bioinformatics and Clinical Sciences, University of Texas Southwestern Medical Center, Dallas, Texas 75390, USA

* correspondence: duojia.pan@utsouthwestern.edu

Abstract:

Many genes that function in animal development are present in the close unicellular relatives of animals, but little is known regarding the premetazoan function of these genes. Here, we develop techniques for genetic manipulation in the filasterean *Capsaspora owczarzaki* and use these tools to characterize the *Capsaspora* ortholog of the Hippo signaling nuclear effector YAP/TAZ/Yorkie (coYki). In contrast to its potent oncogene activity in metazoans, we show that coYki is dispensable for cell proliferation but regulates cytoskeletal dynamics and the morphology of multicellular aggregates in *Capsaspora*. Our results suggest an ancestral role for the Hippo pathway in cytoskeletal regulation, which was later co-opted to regulate cell proliferation in animals.

One Sentence Summary: Gene disruption in a unicellular holozoan suggests an ancestral role for YAP/TAZ/Yorkie in cytoskeletal regulation and cell aggregation but not cell proliferation.

Main text:

The vast morphological diversity observed in animals is generated by developmental programs mediated by a surprisingly small set of conserved signaling pathways (*1*). An exciting and unexpected finding from comparative genomic analysis indicates that many components of these pathways are present in the closest unicellular relatives of animals (*2*). This finding raises the question of whether these genes show similar functions in animals and their unicellular relatives, and, if not, what the ancestral functions of these

genes were, and how they evolved to function in multicellular processes in animals. Answering this question could illuminate the roots of animal multicellularity and provide novel perspective on how to manipulate the activity of these biomedically important pathways.

One such signaling pathway is the Hippo pathway, which coordinates cell proliferation, differentiation, and survival in animals. Initially defined as a tumor suppressor pathway that restricts tissue growth in *Drosophila* development, Hippo signaling plays a conserved role in organ size control and regeneration in mammals *(3, 4)*. This pathway comprises a core kinase cascade involving sequential activation of two kinases, Hpo/MST and Wts/LATS, which culminates in the phosphorylation and inactivation of the potent growth-stimulatory transcriptional coactivator Yorkie/YAP/TAZ (*5*). This core kinase cascade is in turn regulated by diverse upstream inputs, most notably mechanical force, the state of the actin cytoskeleton, and cell-cell or cell-substrate adhesion as part of a mechanotransduction pathway that relays mechanical and architectural cues to gene expression (*6*). Echoing its pervasive function in metazoan growth control, the Hippo pathway is required for contact-inhibition of proliferation in cultured mammalian cells (*7*), and defective Hippo signaling leading to YAP/TAZ oncogene activation is a major driver of human cancers (*8*).

The Hippo pathway was at one point thought to be specific to animals. However, recent genome sequencing efforts have revealed that a core Hippo pathway and many known upstream regulators are encoded in the genomes of the closest unicellular relatives of

63 animals such as choanoflagellates and filasterians (*9*). The choanoflagellates are
64 flagellated filter feeders that can form multicellular rosette structures by incomplete
65 cytokinesis (*10*), whereas filasterians are amoeboid organisms characterized by actin-
66 rich filopodial projections (Fig. 1, A and B) and represent the most basal known unicellular
67 organism encoding all core components of the Hippo pathway (*9*). *Capsaspora*
68 *owczarzaki* is a filasterean originally isolated as a putative endosymbiont in the freshwater
69 snail *B. glabrata* that can attack and kill the parasitic schistosome *S. mansoni* (*11*).
70 *Capsaspora* can be cultured easily in growth medium containing protein source and
71 serum in adherent or shaking culture and can be transiently transfected, allowing for the
72 examination of protein localization using fluorescent fusion proteins (*12*). Although
73 *Capsaspora* tends to grow as a unicellular organism in laboratory culture conditions,
74 under certain conditions *Capsaspora* cells can adhere to each other to form multicellular
75 aggregates (Fig. 1, C to E, (*13*)), suggesting that multicellular behaviors may have been
76 selected for in the lineage leading to *Capsaspora*. Previously, we have shown that
77 overexpression of *Capsaspora* Hippo pathway components such as CoYki and CoHpo in
78 *Drosophila* elicits similar phenotypes as their *Drosophila* counterpart (*9*), suggesting that
79 a biochemically active Hippo signaling pathway likely evolved well before the emergence
80 of Metazoa. Besides the Hippo pathway, the *Capsaspora* genome encodes homologues
81 of other key regulators of animal development such as components of the integrin
82 adhesome (*14*), cadherins (*15*), tyrosine kinases such as Src and Abl (*16*), NF-kB (*17*)
83 and p53 (*18*). Thus, *Capsaspora* offers a unique opportunity to elucidate the ancestral
84 function of these important developmental regulators in a close unicellular relative of
85 animals.

86

87 In an effort to make *Capsaspora* a tractable system for evolutionary cell biology studies,
88 we developed genetic tools for overexpression and loss-of-function analysis. We first
89 established a method for engineering stable *Capsaspora* cell lines by transfecting a vector
90 encoding the fluorescent protein mScarlet and resistance to the antibiotic Geneticin
91 (GenR). After transfection, antibiotic selection, and generation of clonal lines by serial
92 dilution, we were able to generate uniformly mScarlet-positive clonal populations of cells
93 (Fig. 1F**)**. Besides GenR, transfection of *Capsaspora* with genes encoding resistance to
94 nourseothricin (NatR) or hygromycin (HygR) followed by selection with the respective
95 antibiotic could also generate drug-resistant transformants (fig. S1). These results
96 demonstrate that stable *Capsaspora* cell lines expressing multiple transgenes can be
97 generated.

98

99 We next sought to develop tools for loss-of-function analysis in *Capsaspora*. After
100 unsuccessful attempts with CRISPR-Cas9-mediated genome editing, possibly due to the
101 lack of nonhomologous end joining machinery components in *Capsaspora*, we used
102 homologous recombination for gene disruption by replacing each allele of a diploid
103 *Capsaspora* gene with a distinct selectable antibiotic marker (Fig. 1G). This strategy
104 allowed us to generate a cell line in which both *coYki* alleles were disrupted (fig. S2), with
105 no detectable expression of the deleted region of *coYki* **(**Fig. 1, H to J**)**. These results
106 demonstrate the generation of a homozygous *coYki* disruption mutant (subsequently
107 *coYki -/-*) and establish a method for the generation of mutants by gene targeting in
108 *Capsaspora.*

109

110 To determine the effect of loss-of-coYki on cell proliferation, we examined the proliferation
111 of *Capsaspora* cells in adherent or shaking culture. In contrast to what may be expected
112 based on previous studies in animal cells, we observed no significant difference in cell
113 proliferation between WT and *coYki -/-* cells in either condition (Fig. S3). We next sought
114 to examine cell proliferation within *Capsaspora* aggregates. Previously, aggregates have
115 been generated by gentle shaking of cell cultures (*13*). To make aggregates more
116 amenable to extended imaging *in situ*, we developed a condition that induced robust
117 aggregate formation by plating *Capsaspora* cells in low-adherence wells (Fig. 1, C to E).
118 Under this condition, most cells coalesced into aggregates over 2-3 days, leaving few
119 isolated cells in the culture. Treatment with the calcium chelator EGTA resulted in rapid
120 dissociation of the aggregates (fig. S4), suggesting that calcium-dependent cell adhesion
121 mediates aggregate integrity. We used EdU incorporation to label proliferating cells in
122 aggregates, and observed no significant difference in the percent of EdU-positive cells
123 between WT and *coYki -/-* genotypes (Fig. 2, A and B). Unlike clones of cultured
124 mammalian cells that often display increased cell proliferation at the clonal boundary (*19*),
125 distribution of EdU+ cells was homogeneous within *Capsaspora* aggregates (Fig. 2A),
126 suggesting that a mechanism akin to contact-mediated inhibition of proliferation is absent
127 in *Capsaspora*. Together, these results suggest that the rate of proliferation of
128 *Capsaspora* is independent of YAP/TAZ/Yorkie or contact inhibition.

129

130 While examining *Capsaspora* aggregates, we observed a profound phenotype in the
131 shape of the *coYki -/-* aggregates. After aggregate induction by plating cells in low-

132 adherence conditions, WT cell aggregates showed a round morphology (Fig. 2C). In
133 contrast, *coYki -/-* aggregates were asymmetric and less circular than WT aggregates
134 (Fig. 2D). Computational analysis of aggregate morphology and size revealed that WT
135 and *coYki -/-* aggregate size was not significantly different (Fig. 2E), whereas *coYki -/-*
136 aggregates were significantly less circular than WT aggregates (Fig. 2F). Optical
137 sectioning of aggregates expressing mScarlet showed that WT aggregates were thicker
138 perpendicular to the culture surface and more spherical than *coYki -/-* aggregates (Fig.
139 2G). Time-lapse microscopy of aggregation over a period of six days showed that,
140 whereas WT cells accreted into round aggregates that fused with other aggregates when
141 in close proximity but never underwent fission, *coYki -/-* aggregates were dynamically
142 asymmetrical, showed a progressive reduction in circularity, and occasionally underwent
143 fission (movie S1). Taken together, these findings uncover a critical role for coYki in social
144 interactions underlying aggregate morphology, but not cell proliferation, in *Capsaspora*.
145
146 Cell-cell adhesion and cell-substrate adhesion affect the morphology and stability of
147 tumor cell aggregates (*20, 21*). We therefore tested whether cell-cell adhesion and cell-
148 substrate adhesion differ in WT *and coYki -/- cells.* A prediction of differential cell-cell
149 adhesion is that mosaic aggregates of WT and *coYki -/-* cells may show cell sorting within
150 aggregates (*22*). To test this prediction, we induced aggregate formation after mixing
151 mCherry-labeled WT or *coYki* -/- cells with unlabeled WT cells at 1:9 ratio. The distribution
152 of mCherry-labeled WT or *coYki* -/- cells within such mixed aggregates was similar and
153 no cell sorting was evident (fig. S5)**,** indicating that individual *coYki -/-* cells are competent
154 to adhere to and integrate within aggregates and suggesting that the aberrant morphology

155 of *coYki -/-* aggregates is an emergent property of a large number of *coYki -/-* cells. To
156 further test whether cell-cell adhesion differs in WT and *coYki -/-* cells, we vigorously
157 vortexed *Capsaspora* culture to separate individual cells, allowed cell clumps to form by
158 cell-cell adhesion under gentle rotation, and then counted the number of cells in each
159 clump. Numbers of cells per clump were similar for WT and *coYki -/-* cells (fig. S6A),
160 suggesting that the occurrence of cell-cell adhesion is similar in these genotypes. We
161 next tested whether cell-substrate adhesion differed in WT and *coYki -/-* cells by agitating
162 cultures of adherent cells and counting the number of cells that disassociate from the
163 culture surface. After agitation, significantly more *coYki -/-* cells remained attached to the
164 culture surface compared to WT cells (fig. S6B), indicating that coYki negatively regulates
165 cell-substrate adhesion. Together, our data suggest that coYki affects the morphology of
166 cell aggregates by affecting cell-substrate adhesion but not cell-cell adhesion.
167
168 To characterize properties of *coYki -/-* cells that may contribute to abnormal aggregate
169 morphology, we used time-lapse microscopy to examine the dynamic morphology of
170 individual WT and *coYki -/-* cells in adherent culture. Interestingly, the cortices of *coYki -*
171 */-* cells were much more dynamic than those of WT cells. Whereas *coYki -/-* cells display
172 extensive membrane protrusions and retractions, such dynamic membrane structures
173 were rarely observed in WT cells (movie S2). To characterize the differences in cell
174 membrane dynamics, we quantified the occurrence of cell protrusions in WT cells, *coYki*
175 *-/-* cells, and *coYki -/-* cells expressing a *coYki* rescue transgene. WT cells rarely showed
176 protrusions. In contrast, *coYki -/-* cells showed an average of 3.1 protrusions per minute
177 (Fig. 3A), a phenotype that was rescued in *coYki -/-* cells expressing a *coYki* transgene

178 (Fig. 3A, movie S3). These results suggest that coYki affects the cortical dynamics of
179 *Capsaspora* cells.
180
181 In principle, the extensive membrane protrusions made by *coYki -/-* cells may represent
182 F-actin-rich pseudopodia, which drive amoeboid motility, or, alternatively, F-actin-poor
183 blebs, which are actin-depleted extensions of plasma membrane generated by
184 disassociation of the membrane from the cell cortex or cortical rupture (*23*). To distinguish
185 between these possibilities, we stably expressed a fusion protein of the F-actin-binding
186 Lifeact peptide (*24*) with mScarlet in WT and *coYki -/-* cells and examined F-actin
187 dynamics by time-lapse microscopy in adherent cells. At the basal side of WT cells,
188 Lifeact-mScarlet was often enriched at the cell edge corresponding to the direction of cell
189 movement, suggesting that *Capsaspora* undergoes F-actin-mediated amoeboid
190 locomotion (movie S4)**.** As cells move, some Lifeact-mScarlet signal appears as
191 stationary foci on the basal surface, suggesting the existence of actin-rich structures that
192 mediate cell-substrate interaction in *Capsaspora* (Fig. 3B, movie S4). Optical sections at
193 mid-height of WT cells showed that F-actin was enriched at a circular cell cortex, where
194 transient bursts of small F-actin puncta were often observed (Fig. 3B, movie S5). In
195 contrast, cortical shape was less circular in *coYki -/-* cells, and F-actin concentration along
196 the cortex was less uniform (Fig. 3B). During the formation of the membrane protrusions
197 produced by *coYki -/-* cells, F-actin was initially depleted as compared to the rest of the
198 cell (Fig. 3C, movie S6). After the membrane protrusions had fully extended, F-actin
199 accumulated first at the distal end and then along the entire cortex of the protrusion,
200 followed by the regression of the protrusion. A similar sequence of cytoskeletal events

occurs in blebbing mammalian cells (*25*). These results suggest that the protrusions observed in *coYki -/-* cells are actin-depleted blebs, and that after bleb formation, F-actin re-accumulates within the bleb leading to cortical reformation and bleb regression.

To determine whether the abnormal cortical cytoskeleton is specific to *coYki -/-* cells in adherent culture, we examined *coYki -/-* cells within aggregates by time-lapse microscopy. Lifeact-mScarlet-expressing cells were mixed with cells stably expressing the green fluorescent protein Venus so that Lifeact-mScarlet-expressing cells were well-spaced and able to be imaged individually. As in adherent cells, *coYki -/-* cells within aggregates showed dynamic formation of actin-depleted blebs (movie S7). Thus, *coYki -/-* cells show aberrant cortical cytoskeleton and excessive membrane blebbing in both isolated adherent cells and within aggregates.

Loss of coYki causes both bleb-like protrusions and abnormal aggregate morphology, suggesting that the cellular phenotypes observed in *coYki -/-* cells (membrane blebbing and related cortical cytoskeletal defects) may underlie the aberrant aggregate morphology. We tested this hypothesis by treating *coYki -/-* cells with Blebbistatin, a myosin II inhibitor named after its bleb-inhibiting activity in mammalian cells (*26*). Strikingly, not only did low concentrations of Blebbistatin suppress the formation of blebs in *coYki -/-* cells (Fig. 3D, movie S8), Blebbistatin also rescued the abnormal morphology of *coYki -/-* aggregates (Fig. 3E). Whereas *coYki -/-* cell aggregates were asymmetric and showed low circularity (Fig. 3E'''), *coYki -/-* aggregates treated with blebbistatin were circular and resembled WT aggregates (Fig. 3E'''' and 3F). These results suggest a

224 causal link between the membrane/cytoskeletal defects observed in individual *coYki -/-*
225 cells and the abnormal morphology of *coYki -/-* aggregates.
226
227 To characterize the transcriptional targets of coYki that may underlie the
228 morphological/cytoskeletal defects of *coYki -/-* cells, we performed RNAseq on WT and
229 *coYki -/-* cells in adherent culture. This analysis revealed 1205 differentially expressed
230 genes, including 397 downregulated and 808 upregulated genes in the *coYki* mutant.
231 Functional enrichment analysis of these two gene sets revealed distinct enrichment of
232 functional categories (Fig. 4, A and B). Genes predicted to encode actin-binding proteins
233 were enriched in the set of genes upregulated in the *coYki -/-* mutant, suggesting that
234 these genes may play a role in the aberrant cytoskeletal dynamics observed in *coYki -/-*
235 *cells.* To further inquire into the potential function of coYki-regulated genes, we searched
236 the 1205 differentially expressed genes against a previously reported *Capsaspora*
237 phylome (*27*) to identify 638 *Capsaspora* genes with predicted human or mouse
238 orthologs. Ingenuity Pathway Analysis of this mammalian ortholog set showed that the
239 two most significantly enriched functional categories corresponded to cell movement and
240 cell migration (Fig. 4C). Notably, regulation of cell migration was reported as the most
241 enriched functional category among YAP target genes in glioblastoma cells (*28*), and cell
242 motility was an enriched category in an integrative analysis of gene regulatory networks
243 downstream of YAP/TAZ utilizing transcriptomic and cistromic data from multiple human
244 tissues (*29*). However, in contrast to functional enrichment studies in metazoan systems
245 examining genes regulated by Yorkie/YAP/TAZ (*28, 30, 31*), no enrichment was detected

246 in functional categories of cell proliferation or the cell cycle (Fig. 4C). This finding is
247 consistent with the lack of a proliferative phenotype in *coYki -/-* cells.
248
249 In summary, we show that coYki regulates cytoskeletal dynamics and potentially other
250 cortical actin-related processes but is dispensable for the proliferation of *Capsaspora*
251 cells. Such coYki-dependent cortical cytoskeletal function, in turn, regulates the
252 morphology of *Capsaspora* aggregates in a manner that may involve tuning the strength
253 of cell-substrate adhesion. Although the natural history of *Capsaspora*, including the
254 selective advantage of cell aggregation, is poorly understood, our findings suggest that
255 cytoskeletal regulation represents an ancestral function of the Hippo pathway predating
256 the origin of Metazoa, and this pathway was later co-opted to control cell proliferation
257 after the unicellular-to-multicellular transition. Given that the cortical cytoskeleton is both
258 an important upstream regulator and a downstream effector of Hippo signaling in animal
259 cells (*32, 33*), the co-option of the Hippo pathway for cell proliferation control in early
260 metazoans may have provided a convenient mechanism that couples cell proliferation
261 with cytoskeletal and mechanical properties of the cells. Besides illuminating an ancestral
262 function of the Hippo pathway, the genetic tools we have developed for modifying the
263 *Capsaspora* genome provide an unprecedented opportunity to interrogate the
264 premetazoan functions of other developmental regulators that are present in the genomes
265 of close unicellular relatives of animals.
266
267 **References and Notes:**

268 1. A. Pires-daSilva, R. J. Sommer, The evolution of signalling pathways in animal
269 development. *Nat Rev Genet* **4**, 39-49 (2003).

270 2. N. Ros-Rocher, A. Perez-Posada, M. M. Leger, I. Ruiz-Trillo, The origin of
271 animals: an ancestral reconstruction of the unicellular-to-multicellular transition.
272 *Open Biol* **11**, 200359 (2021).

273 3. S. Wu, J. Huang, J. Dong, D. Pan, hippo encodes a Ste-20 family protein kinase
274 that restricts cell proliferation and promotes apoptosis in conjunction with
275 salvador and warts. *Cell* **114**, 445-456 (2003).

276 4. K. F. Harvey, C. M. Pfleger, I. K. Hariharan, The Drosophila Mst ortholog, hippo,
277 restricts growth and cell proliferation and promotes apoptosis. *Cell* **114**, 457-467
278 (2003).

279 5. J. Huang, S. Wu, J. Barrera, K. Matthews, D. Pan, The Hippo signaling pathway
280 coordinately regulates cell proliferation and apoptosis by inactivating Yorkie, the
281 Drosophila Homolog of YAP. *Cell* **122**, 421-434 (2005).

282 6. Y. Zheng, D. Pan, The Hippo Signaling Pathway in Development and Disease.
283 *Dev Cell* **50**, 264-282 (2019).

284 7. B. Zhao *et al.*, Inactivation of YAP oncoprotein by the Hippo pathway is involved
285 in cell contact inhibition and tissue growth control. *Genes Dev* **21**, 2747-2761
286 (2007).

287 8. Y. Wang *et al.*, Comprehensive Molecular Characterization of the Hippo
288 Signaling Pathway in Cancer. *Cell Rep* **25**, 1304-1317 e1305 (2018).

289 9. A. Sebe-Pedros, Y. Zheng, I. Ruiz-Trillo, D. Pan, Premetazoan origin of the hippo
290 signaling pathway. *Cell Rep* **1**, 13-20 (2012).

291 10. S. R. Fairclough, M. J. Dayel, N. King, Multicellular development in a
292 choanoflagellate. *Curr Biol* **20**, R875-876 (2010).

293 11. H. H. Stibbs, A. Owczarzak, C. J. Bayne, P. DeWan, Schistosome sporocyst-
294 killing Amoebae isolated from Biomphalaria glabrata. *J Invertebr Pathol* **33**, 159-
295 170 (1979).

296 12. H. Parra-Acero *et al.*, Transfection of Capsaspora owczarzaki, a close unicellular
297 relative of animals. *Development* **145**, (2018).

298 13. A. Sebe-Pedros *et al.*, Regulated aggregative multicellularity in a close unicellular
299 relative of metazoa. *Elife* **2**, e01287 (2013).

300 14. A. Sebe-Pedros, A. J. Roger, F. B. Lang, N. King, I. Ruiz-Trillo, Ancient origin of
301 the integrin-mediated adhesion and signaling machinery. *Proc Natl Acad Sci U S*
302 *A* **107**, 10142-10147 (2010).

303 15. S. A. Nichols, B. W. Roberts, D. J. Richter, S. R. Fairclough, N. King, Origin of
304 metazoan cadherin diversity and the antiquity of the classical cadherin/beta-
305 catenin complex. *Proc Natl Acad Sci U S A* **109**, 13046-13051 (2012).

306 16. H. Suga *et al.*, Genomic survey of premetazoans shows deep conservation of
307 cytoplasmic tyrosine kinases and multiple radiations of receptor tyrosine kinases.
308 *Sci Signal* **5**, ra35 (2012).

309 17. L. M. Williams, T. D. Gilmore, Looking Down on NF-kappaB. *Mol Cell Biol* **40**,
310 (2020).

311 18. A. Sebe-Pedros, B. M. Degnan, I. Ruiz-Trillo, The origin of Metazoa: a unicellular
312 perspective. *Nat Rev Genet* **18**, 498-512 (2017).

313 19. H. W. Fisher, J. Yeh, Contact inhibition in colony formation. *Science* **155**, 581-
314 582 (1967).

315 20. A. F. Blandin *et al.*, Glioma cell dispersion is driven by alpha5 integrin-mediated
316 cell-matrix and cell-cell interactions. *Cancer Lett* **376**, 328-338 (2016).

317 21. L. Saias, A. Gomes, M. Cazales, B. Ducommun, V. Lobjois, Cell-Cell Adhesion
318 and Cytoskeleton Tension Oppose Each Other in Regulating Tumor Cell
319 Aggregation. *Cancer Res* **75**, 2426-2433 (2015).

320 22. R. A. Foty, M. S. Steinberg, The differential adhesion hypothesis: a direct
321 evaluation. *Dev Biol* **278**, 255-263 (2005).

322 23. G. Charras, E. Paluch, Blebs lead the way: how to migrate without lamellipodia.
323 *Nat Rev Mol Cell Biol* **9**, 730-736 (2008).

324 24. J. Riedl *et al.*, Lifeact: a versatile marker to visualize F-actin. *Nat Methods* **5**, 605-
325 607 (2008).

326 25. G. T. Charras, C. K. Hu, M. Coughlin, T. J. Mitchison, Reassembly of contractile
327 actin cortex in cell blebs. *J Cell Biol* **175**, 477-490 (2006).

328 26. A. F. Straight *et al.*, Dissecting temporal and spatial control of cytokinesis with a
329 myosin II Inhibitor. *Science* **299**, 1743-1747 (2003).

330 27. A. Sebe-Pedros *et al.*, High-Throughput Proteomics Reveals the Unicellular
331 Roots of Animal Phosphosignaling and Cell Differentiation. *Dev Cell* **39**, 186-197
332 (2016).

333 28. C. Stein *et al.*, YAP1 Exerts Its Transcriptional Control via TEAD-Mediated
334 Activation of Enhancers. *PLoS Genet* **11**, e1005465 (2015).

335 29. M. Paczkowska *et al.*, Integrative pathway enrichment analysis of multivariate
336 omics data. *Nat Commun* **11**, 735 (2020).

337 30. A. Ikmi *et al.*, Molecular evolution of the Yap/Yorkie proto-oncogene and
338 elucidation of its core transcriptional program. *Mol Biol Evol* **31**, 1375-1390
339 (2014).

340 31. F. Zanconato *et al.*, Genome-wide association between YAP/TAZ/TEAD and AP-
341 1 at enhancers drives oncogenic growth. *Nat Cell Biol* **17**, 1218-1227 (2015).

342 32. H. Deng *et al.*, Spectrin couples cell shape, cortical tension, and Hippo signaling
343 in retinal epithelial morphogenesis. *J Cell Biol* **219**, (2020).

344 33. B. G. Fernandez *et al.*, Actin-Capping Protein and the Hippo pathway regulate F-
345 actin and tissue growth in Drosophila. *Development* **138**, 2337-2346 (2011).

346 34. H. Parra-Acero *et al.*, Integrin-Mediated Adhesion in the Unicellular Holozoan
347 Capsaspora owczarzaki. *Curr Biol* **30**, 4270-4275 e4274 (2020).

348 35. D. S. Bindels *et al.*, mScarlet: a bright monomeric red fluorescent protein for
349 cellular imaging. *Nat Methods* **14**, 53-56 (2017).

350 36. D. M. Veltman, G. Akar, L. Bosgraaf, P. J. Van Haastert, A new set of small,
351 extrachromosomal expression vectors for Dictyostelium discoideum. *Plasmid* **61**,
352 110-118 (2009).

353 37. S. S. Lehman *et al.*, Versatile nourseothricin and streptomycin/spectinomycin
354 resistance gene cassettes and their use in chromosome integration vectors. *J*
355 *Microbiol Methods* **129**, 8-13 (2016).

356 38. S. H. Park *et al.*, Generation and application of new rat monoclonal antibodies
357 against synthetic FLAG and OLLAS tags for improved immunodetection. *J*
358 *Immunol Methods* **331**, 27-38 (2008).

359 39. S. J. Charette, P. Cosson, Preparation of genomic DNA from Dictyostelium
360 discoideum for PCR analysis. *Biotechniques* **36**, 574-575 (2004).

361 40. S. Andrews, FastQC: a quality control tool for high throughput sequence data. .
362 *Available online at: http://www.bioinformatics.babraham.ac.uk/projects/fastqc*,
363 (2010).

364 41. S. Wingett, FastQ Screen: quality control tool to screen a library of sequences in
365 FastQ format against a set of sequence databases. . *Available online at:*
366 *http://www.bioinformatics.babraham.ac.uk/projects/fastq_screen*, (2011).

367 42. A. Dobin *et al.*, STAR: ultrafast universal RNA-seq aligner. *Bioinformatics* **29**, 15-
368 21 (2013).

369 43. Y. Liao, G. K. Smyth, W. Shi, featureCounts: an efficient general purpose
370 program for assigning sequence reads to genomic features. *Bioinformatics* **30**,
371 923-930 (2014).

372 44. M. D. Robinson, D. J. McCarthy, G. K. Smyth, edgeR: a Bioconductor package
373 for differential expression analysis of digital gene expression data. *Bioinformatics*
374 **26**, 139-140 (2010).

375 45. J. Huerta-Cepas, S. Capella-Gutierrez, L. P. Pryszcz, M. Marcet-Houben, T.
376 Gabaldon, PhylomeDB v4: zooming into the plurality of evolutionary histories of a
377 genome. *Nucleic Acids Res* **42**, D897-902 (2014).

46. E. Paradis, K. Schliep, ape 5.0: an environment for modern phylogenetics and evolutionary analyses in R. *Bioinformatics* **35**, 526-528 (2019).

47. A. Kramer, J. Green, J. Pollard, Jr., S. Tugendreich, Causal analysis approaches in Ingenuity Pathway Analysis. *Bioinformatics* **30**, 523-530 (2014).

48. W. Huang da, B. T. Sherman, R. A. Lempicki, Bioinformatics enrichment tools: paths toward the comprehensive functional analysis of large gene lists. *Nucleic Acids Res* **37**, 1-13 (2009).

Acknowledgements:

We thank the McDermott Sequencing Core and the Next-Generation Sequencing Core for RNA sequencing, and Dr. Iñaki Ruiz-Trillo for sharing information on *Capsaspora* vectors.

Funding: This work was supported in part by National Institute of Health grant EY015708 to D.P. During this work J.E.P was a Howard Hughes Medical Institute fellow of the Life Sciences Research Foundation. D.P. is an investigator of the Howard Hughes Medical Institute.

Author Contributions: JEP and DP conceived the study and designed experiments. JEP and MS performed experiments. JEP, MK, and CX analyzed RNAseq data. JEP, DP, and MK wrote the original manuscript draft. JEP, MS, DP, MK, and CX revised and edited the manuscript.

Competing interests: Authors declare that they have no competing interests.

403 **Data and materials availability:** RNAseq data generated in this study have been
404 deposited into the NCBI SRA (Bioproject PRJNA759885). The following plasmids have
405 been deposited at Addgene: pJP72 (#176479), pJP102 (#176480), pJP103 (#176481),
406 and pJP118 (#176494).
407
408

Supplementary Materials

Materials and methods

Figs. S1 to S6

References 34 to 48

Movies S1 to S8

Data S1 to S3

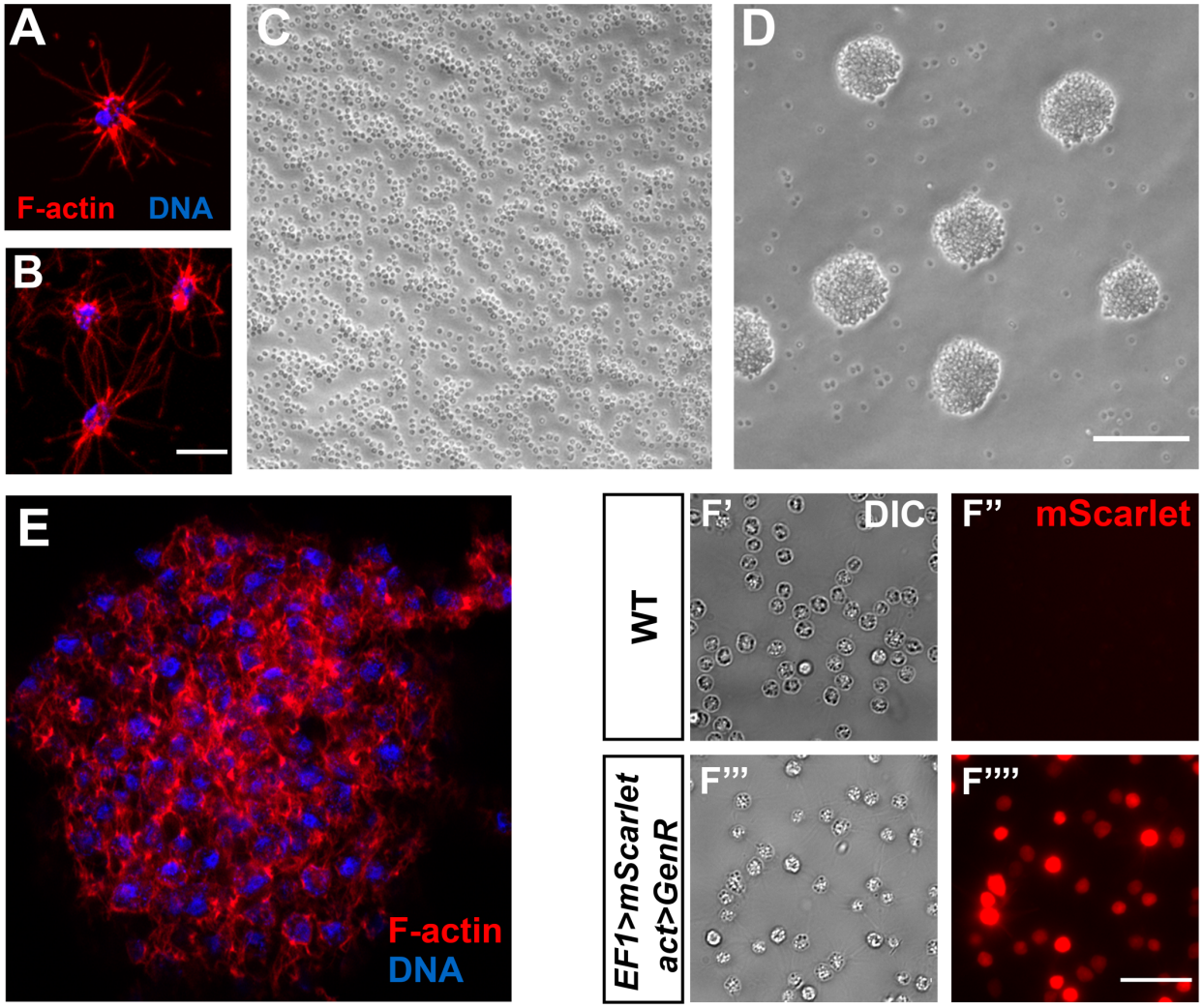
A
F-actin
DNA
B
C
D
E
F-actin
DNA
WT
F'
DIC
F''
mScarlet
EF1>mScarlet
act>GenR
F'''
F''''

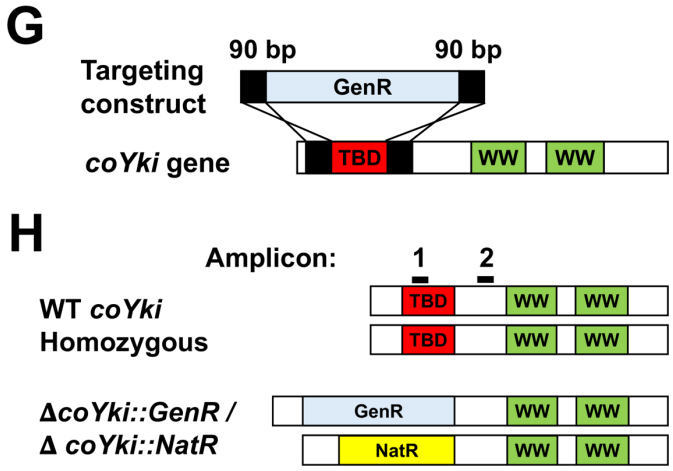
G
Targeting construct
90 bp
90 bp
GenR
coYki gene
TBD
WW
WW
H
Amplicon:
1
2
WT coYki Homozygous
TBD
WW
WW
ΔcoYki::GenR /
Δ coYki::NatR
GenR
NatR
WW
WW

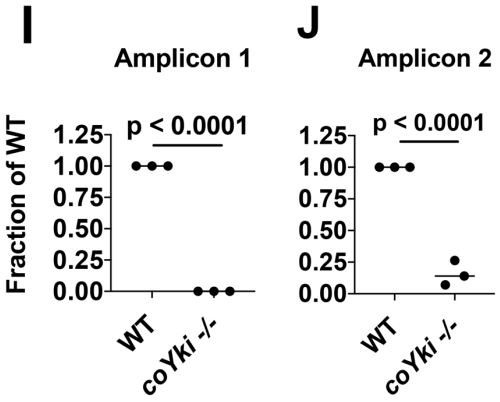
I
Amplicon 1
J
Amplicon 2
Fraction of WT
p < 0.0001
1.25
1.00
0.75
0.50
0.25
0.00
WT
coYki -/-

416

417

418 **Fig. 1. Stable transgene expression and gene knockout in *Capsaspora*. (A)** A solitary
419 *Capaspora* cell showing thin F-actin-enriched projections. Phalloidin and DAPI are used
420 to stain F-actin and DNA, respectively. **(B)** Cells at higher densities can contact other cells
421 through projections. Scale bar is 5 microns. **(C-D)** *Capsapsora* cells were diluted to 7.5 x
422 10^5 cells/mL and inoculated into either a standard polystyrene culture plate **(C)** or a low-
423 adherence plate **(D).** At 3 days, cells in standard plates grow as a monolayer whereas
424 cells in low-adherence plates form round aggregates. **(E)** An aggregate stained for F-actin
425 shows actin-rich connections between cells within an aggregate. Scale bar is 10 microns.
426 (**F)** WT *Capsaspora* cells and a clonal population of cells stably expressing mScarlet were
427 imaged to show fluorescence. Scale bar is 20 microns. **(G)** Strategy for disrupting the
428 *coYki* gene by homologous recombination. GenR, geneticin resistance cassette; TBD,
429 Tead-binding domain; WW, WW domain. **(H)** Strategy for demonstrating disruption of
430 *coYki* by qPCR. Amplicon 1 corresponds to a region of the *coYki* gene that should be
431 absent in a homozygous mutant, whereas Amplicon 2 corresponds to a segment of the
432 gene 3' of the region targeted for deletion. **(I-J)** qPCR of Amplicons 1 and 2 in WT and
433 putative *coYki -/-* cells. The differences between WT and *coYki -/-* for both Amplicons 1
434 and 2 are significant (t-test).
435
436
437

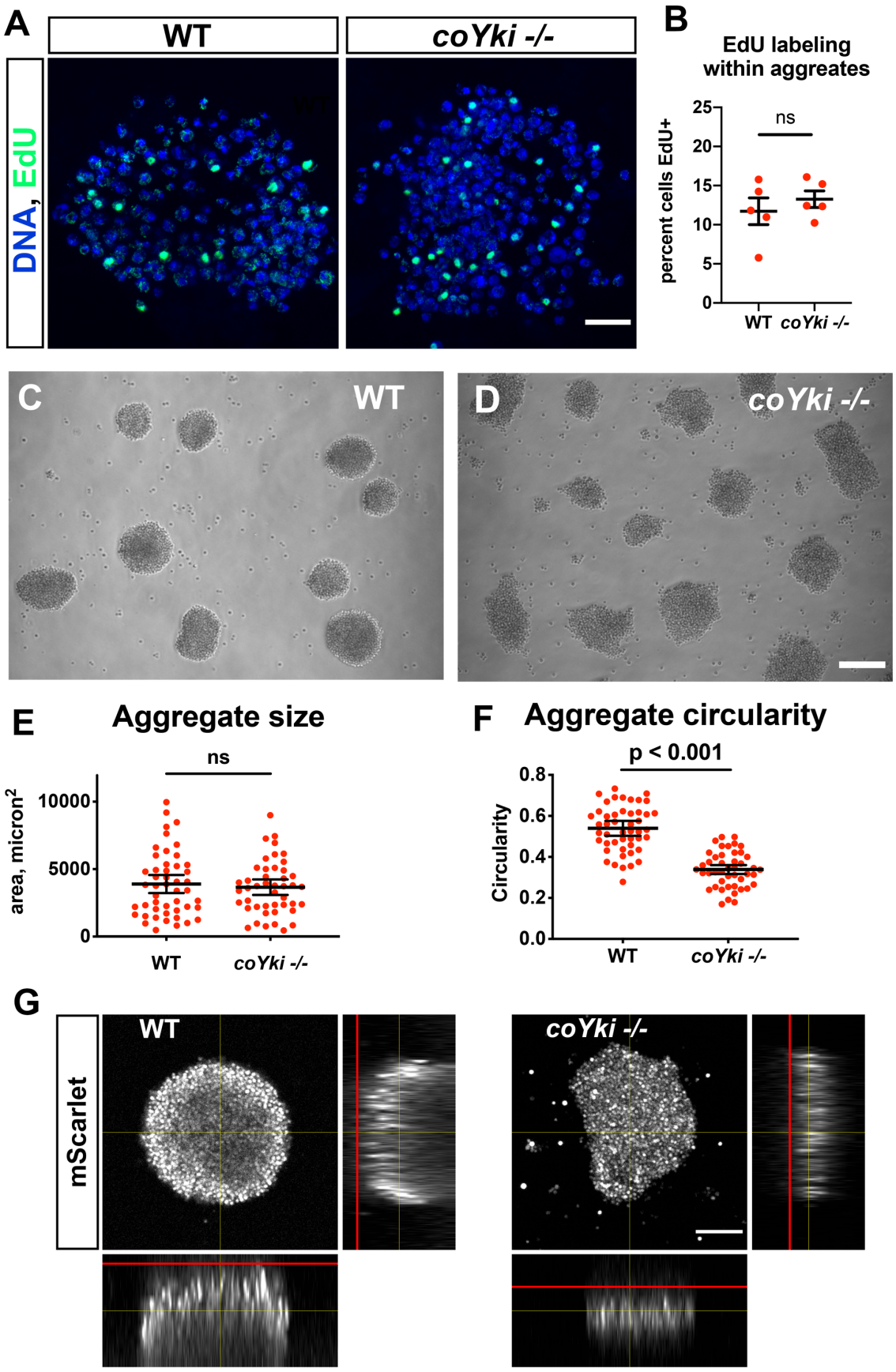
A
WT
coYki -/-
DNA, EdU
B
EdU labeling within aggreates
percent cells EdU+
ns
25
20
15
10
5
0
WT
coYki -/-
C
WT
D
coYki -/-
E
Aggregate size
ns
area, micron2
10000
5000
0
WT
coYki -/-
F
Aggregate circularity
p < 0.001
Circularity
0.8
0.6
0.4
0.2
0.0
WT
coYki -/-
G
mScarlet
WT
coYki -/-

438

Fig. 2. Loss of coYki results in no apparent effect on cell proliferation but alters the morphology of multicellular aggregates. (A) To examine proliferation within aggregates, EdU was used to label proliferating cells within aggregates grown in low-adherence plates. **(B)** The percent of cells positive for EdU within aggregates was quantified. Each red circle indicates measurement results for a single aggregate, and mean ± SEM is shown in black. The difference between WT ant *coYki -/-* cells is not significant (t-test). **(C-D)** WT or *coYki -/-* cells were innoculated into low-adherence plates, and cell aggregates were imaged at 5 days. Scale bar is 75 microns. **(E-F)** Aggregate size and circularity was measured from aggregate images using ImageJ. The difference in aggregate circularity between WT and *coYki -/-* is significant (t-test). Bars indicate the mean ± SEM (n=3 with 15 aggregates measured for each independent experiment), and dots indicate values for individual aggregates. **(G)** Orthogonal views of WT and *coYki -/-* aggregates are shown. Cell aggregates stably expressing mScarlet were imaged live by confocal microscopy. Red lines show the location of the culture surface. Scale bar is 50 microns.

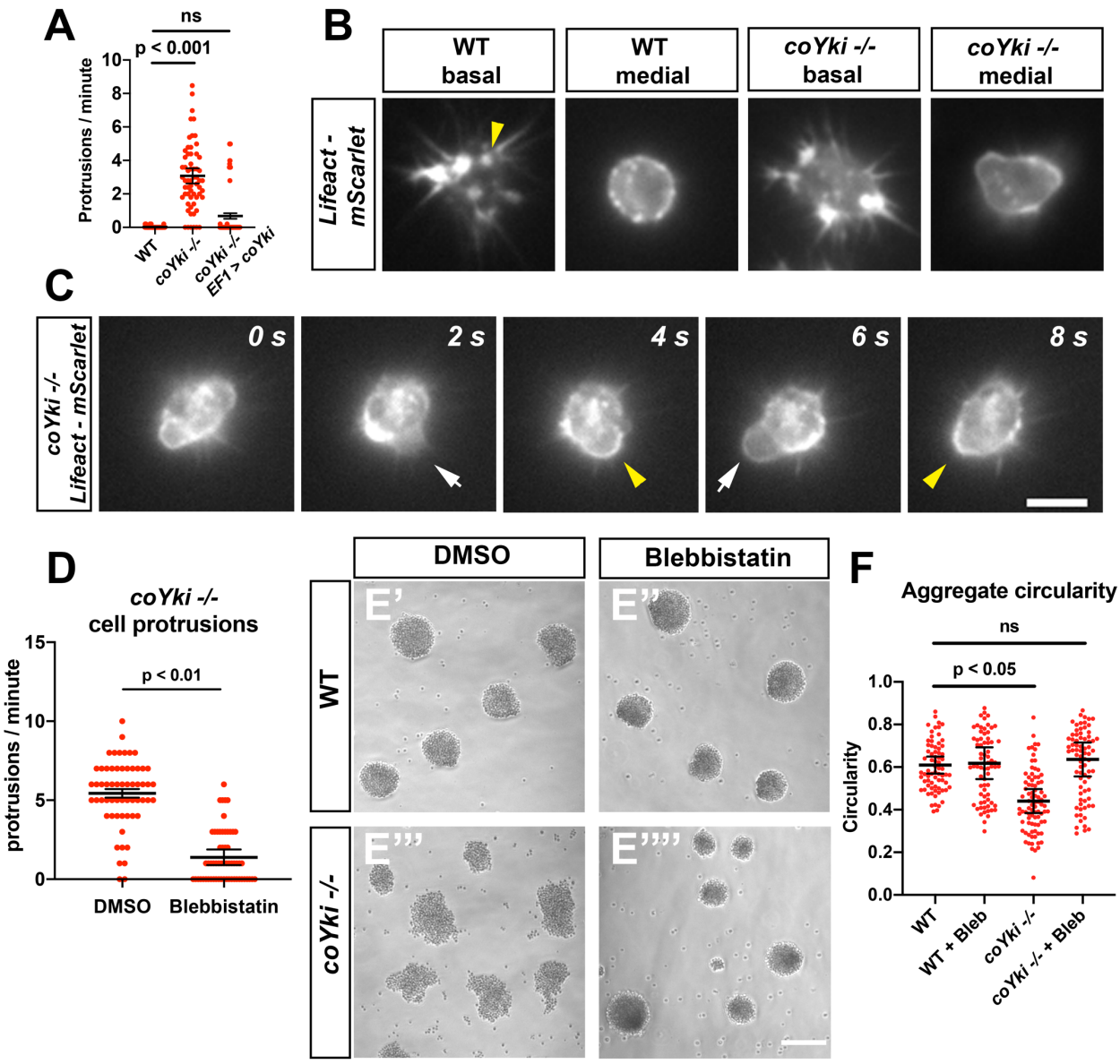

Fig. 3. Loss of coYki results in bleb-like distortions at the cell cortex. (A) *Capsaspora* cells on a glass surface were imaged by time-lapse microscopy and individual cells were scored for number of protrusions per minute. A protrusion is defined as a localized extension of the cell boundary that disrupts a previously inert region of the cortex and/or changes the direction of movement of the cell. Differences between WT and *coYki -/-* are significant (one-way ANOVA, Tukey's test). Values from 3 independent experiments with

465 20 cells measured for each condition per experiment are shown. Red dots indicate the
466 measurement from an individual cell, and black bars indicate the mean ± SEM of the
467 means from each independent experiment. **(B)** Cells on a glass surface stably expressing
468 Lifeact-mScarlet were imaged focusing on the base of the cell at the substrate ("basal")
469 or at the mid-height of the cell ("medial"). Arrowhead shows an example of Lifeact signal
470 at the base of the cell that remains stationary as the cell moves (see Movie S4). Scale
471 bar is 5 microns. **(C)** Time series of a *coYki -/-* cell stably expressing Lifeact-mScarlet on
472 a glass surface. White arrows indicate Lifeact-depleted bleb-like protrusions, and yellow
473 arrowheads indicate areas of cell cortex constriction, which correlate with increased
474 Lifeact signal. Scale bar is 5 microns. **(D)** Cells on a glass surface were treated with
475 DMSO or 1 μM blebbistatin for 1 hour, and then cells were imaged by time lapse
476 microscopy and the number of protrusions per cell was quantified. **(E)** Cells were
477 inoculated into low-adherence plates with DMSO **(E',E''')** or 1 μM blebbistatin **(E'',E'''')**,
478 and aggregates were imaged after 5 days. Scale bar is 75 microns. **(F)** Circularity of
479 aggregates was measured with ImageJ using images of aggregates from the indicated
480 conditions. Black bars indicate the mean ± SEM (n=4 with 15 aggregates measured for
481 each independent experiment), and red dots indicate the measurements for individual
482 aggregates. Differences in circularity between WT and *coYki -/-* aggregates treated with
483 DMSO are significant (one-way ANOVA, Dunnett's test), whereas differences between
484 WT aggregates treated with DMSO and *coYki -/-* aggregates treated with blebbistatin are
485 not. "Bleb" indicates blebbistatin.

486
487

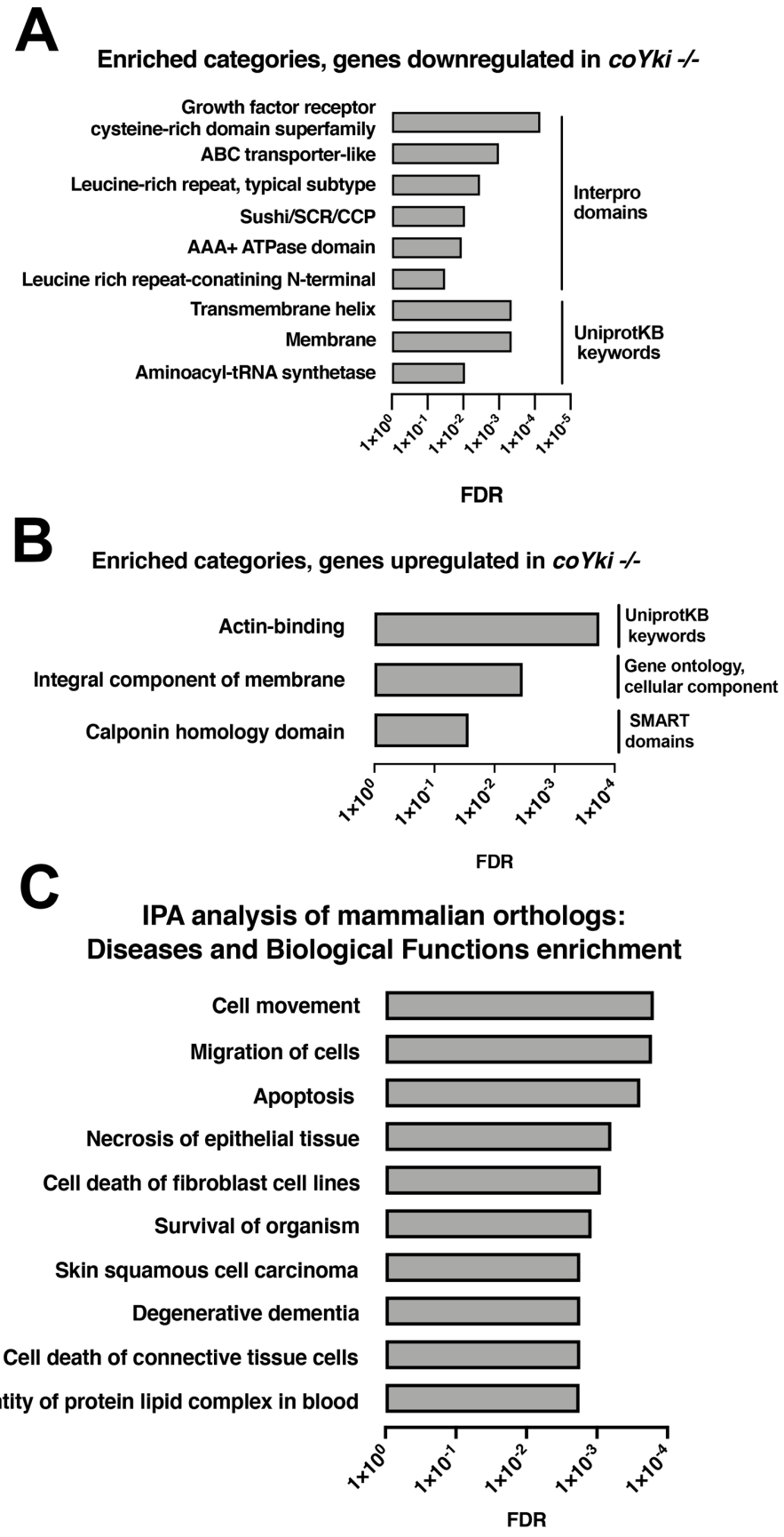
A
Enriched categories, genes downregulated in coYki -/-
Growth factor receptor cysteine-rich domain superfamily
ABC transporter-like
Leucine-rich repeat, typical subtype
Sushi/SCR/CCP
AAA+ ATPase domain
Leucine rich repeat-conatining N-terminal
Transmembrane helix
Membrane
Aminoacyl-tRNA synthetase
Interpro domains
UniprotKB keywords
1×10^0
1×10^-1
1×10^-2
1×10^-3
1×10^-4
1×10^-5
FDR
B
Enriched categories, genes upregulated in coYki -/-
Actin-binding
Integral component of membrane
Calponin homology domain
UniprotKB keywords
Gene ontology, cellular component
SMART domains
1×10^0
1×10^-1
1×10^-2
1×10^-3
1×10^-4
FDR
C
IPA analysis of mammalian orthologs:
Diseases and Biological Functions enrichment
Cell movement
Migration of cells
Apoptosis
Necrosis of epithelial tissue
Cell death of fibroblast cell lines
Survival of organism
Skin squamous cell carcinoma
Degenerative dementia
Cell death of connective tissue cells
Quantity of protein lipid complex in blood
1×10^0
1×10^-1
1×10^-2
1×10^-3
1×10^-4
FDR

488

489

490 **Fig. 4. Functional enrichment of genes differentially expressed in *coYki -/-* cells.**
491 Top enriched categories from the sets of genes significantly downregulated **(A)** or
492 upregulated **(B)** in *coYki -/-* cells compared to WT are shown. **(C)** Ingeneuity Pathway
493 Analysis was performed on a set of predicted human/mouse orthologs of *Capsaspora*
494 genes with significant changes in expression in *coYki -/-* cells. Enriched diseases and
495 biological functions with false discovery rate (FDR) $\leq$ 0.05 are shown.

496

497

Supplementary Materials for

Genome editing of *Capsaspora owczarzaki* suggests an ancestral function of the Hippo signaling effector YAP/TAZ/Yorkie in cytoskeletal dynamics but not proliferation

Jonathan E Phillips, Mohammed Kanchwala, Chao Xing, and Duojia Pan

Correspondence to: duojia.pan@utsouthwestern.edu

This PDF file includes:

Materials and Methods
Figs. S1 to S6
Captions for Movies S1 to S8
Captions for Data S1 to S3

Other Supplementary Materials for this manuscript include the following:

Movies S1 to S8
Data S1 to S3:

Data S1. Sequences of synthesized gene fragments used in this study
Data S2. Sequences of oligonucleotides used in this study
Data S3. Plasmids constructed for this study

529 **Materials and Methods**

530 Cell culture

531 *Capsaspora* cells were maintained in ATCC Medium 1034 (modified PYNFH medium)
532 supplemented with 25 µg/mL Ampicillin (referred to below as "growth medium") in a 23°C
533 incubator. Cells were kept in either 25 cm^2 cell culture flasks in 8 mL medium or in 75 cm^2
534 cell culture flasks in 15 ml medium. To induce cell aggregation, cells were resuspended
535 to 7.5 x 10^5 cells/ml in growth medium, and 1 ml of this cell suspension was added per
536 well to a 24-well ultra-low attachment plate (Sigma CLS3473). To test the effect of
537 blebbistatin on aggregate morphology, a 20 mM stock solution of blebbistatin (Sigma
538 B0560) in DMSO was made, and cells were resuspended to 7.5 x 10^5 cells/ml in growth
539 medium with 1 µm blebbistatin or DMSO only as a vehicle control. Aggregates were then
540 generated as described above and imaged with a Nikon Eclipse Ti inverted microscope
541 with NIS-Elements acquisition software.

542

543 To characterize cell proliferation during growth on a solid substrate, *Capsaspora* cells
544 were diluted to 1 x 10^5 cells/ml in growth medium, and 800 µl of this dilution was pipetted
545 into multiple wells in a 24-well polystyrene cell culture plate. To prevent edge effects,
546 wells at the edge of the plate were not used and were instead filled with 800 µl of water.
547 The plates were then kept in in a 23°C incubator. Each day, 1.5 µl of a 500 mM EDTA
548 solution was added to a well, and cells in the well were resuspended by pipetting up and
549 down for one minute. Resuspended cells were then transferred to a 1.5 mL tube,
550 vortexed, and then the cell density was determined by hemocytometer. To characterize
551 cell proliferation in shaking culture, cells were diluted to 1 x 10^5 cells/ml in growth medium,

552 and 20 ml of this dilution was added to a 125 ml Erlenmeyer culture flask. Cultures were
553 then incubated in an orbital shaker at 150 rpm and 23°C. Cell density was determined
554 daily by transferring 200 µl of culture to a 1.5 ml tube, adding 1.5 µl of 500 mM EDTA
555 solution to disassociate any aggregated cells, vortexing, and counting by hemocytometer.
556

557 Fixation and staining of aggregates

558 To fix and stain aggregates, aggregates were generated as described above, and then
559 aggregates were collected from a 24-well plate by gentle pipetting. 500 µl of aggregate
560 suspension was added dropwise to 9 ml of PM PFA (100 mM PIPES ph 6.9, 0.1 mM
561 $MgSO_4$, 4% PFA filtered through a 0.45 µm syringe filter) in a 15 mL polystyrene tube,
562 and tubes were left undisturbed for 1 hour to allow fixation. Aggregates were then
563 centrifuged at 1000 x g for 3 minutes and resuspended in 500 µl of PEM buffer (100 mM
564 PIPES pH 6.9, 1 mM EGTA, 0.1 mM $MgSO_4$). After transferring aggregates to a
565 microcentrifuge tube, aggregates were centrifuged for 2000 x g for 2 minutes, the
566 supernatant was removed, and aggregates were resuspended in 300 µl of PEM.
567

568 As we found that aggregates were fragile during continued centrifugation-resuspension
569 cycles, we developed a protocol where solution changes could be done without
570 centrifugation using 24-well plate inserts with an 8 micron pore membrane at the insert
571 base (Corning 3422). Before use with aggregates, 100 µl PEM buffer was added to a well
572 in a 24-well plate, 300 µl of PEM was added to a membrane insert, and the insert was
573 placed in the well and allowed to drain (contact between the membrane and the solution
574 within the well is critical for draining). Aggregates in 300 µl of PEM were added to the

575 insert, and the insert was moved to a new well with 100 µl of PEM and allowed to drain.
576 As a wash step, the membrane insert was then moved to a well containing 1200 µl of
577 PEM, allowing the membrane insert to fill with PEM buffer, and after a 5 minute incubation,
578 the membrane was moved to a new well with 100 µl of PEM and allowed to drain. The
579 membrane insert was then moved to a well containing 1200 µl of PEM
580 block/permeabilization solution (100 mM PIPES pH 6.9, 1 mM EGTA, 0.1 mM $MgSO_4$,
581 1% BSA, 0.3% Triton X-100) and incubated for 30 minutes at room temperature. The
582 membrane insert was moved to a well with 100 µl of PEM and allowed to drain and then
583 moved into a well containing 1 mL PEM with DAPI (2 µg/mL) and Phalloidin (0.1 µM) and
584 incubated for 15 minutes at room temperature. Aggregates were then washed once more
585 in 1200 µl PEM. To mount aggregates for imaging, the membrane insert was placed in a
586 new well with 100 µl of PEM buffer and was allowed to drain, aggregates were
587 resuspended in the residual buffer (approximately 50 µl) by gentle pipetting, and then
588 aggregates were pipetted onto a microscope slide and allowed to settle for 5 minutes.
589 Kimwipes were then placed in contact with the edge of the liquid on the slide, allowing for
590 removal of excess buffer by capillary action. 15 µl of Fluoromount G (SouthernBiotech)
591 was pipetted onto the aggregates, which were then covered with a 22 x 40 mm cover
592 glass and sealed with nail polish. Aggregates were subsequently imaged with a Zeiss
593 LSM 880 confocal microscope. Staining of adherent cells with phalloidin was done as
594 previously described (*34*).
595
596 <u>EdU labeling of aggregates</u>

597 To examine cell proliferation within aggregates by EdU labeling, aggregates were
598 generated in ultra-low adherence 24-well plates as described above. 3 days after
599 aggregation was initiated, 100 µl of growth medium containing EdU was added to
600 aggregates to result in a 150 µM EdU concentration. Aggregates were incubated with
601 EdU for 4 hours and then fixed and resuspended in 300 µl PEM buffer as described
602 above. Aggregates were then processed for imaging following the manufacturer's
603 protocol (ThermoFisher C10339) using the 24-well plate membrane insert method
604 described above to transfer aggregates between solutions. For all steps, wells with 1 mL
605 of solution were used for washing or staining cells in membrane inserts, and wells with
606 100 µl of solution were used to drain wells in preparation for transfer into the next solution.
607

608 Molecular Biology

609 For the sequences of synthesized DNA fragments and oligonucleotides used in this study,
610 see Data S1 and S2, respectively. For a list of plasmids generated for this study, see Data
611 S3. To generate a vector for mScarlet expression in *Capsaspora* (pJP71), a DNA
612 construct containing an open reading frame encoding the mScarlet protein (*35*) codon-
613 optimized for expression in *Capsaspora* and under control of the previously described
614 EF1-α promoter and terminator from the pONSY-mCherry vector (*12*) was constructed by
615 gene synthesis (sJP1) and cloned into the EcoRV site of the pUC57-mini vector
616 (Genscript). A KpnI site and an AflII site were incorporated at the beginning and end of
617 the coding sequence, respectively, allowing for the construction of N or C-terminal protein
618 fusion constructs by Gibson assembly. To generate a plasmid for expression of mScarlet
619 and a Geneticin resistance gene (pJP72), the NeoR coding sequence from the

620 *Dictyostelium* pDM323 vector (*36*) was codon optimized for *Capsaspora*, the optimized
621 sequence was synthesized with the promoter and terminator from the *Capsaspora* actin
622 ortholog gene CAOG_06018, and the synthesized fragment (sJP2) was cloned into the
623 SmaI site of pJP71 by Gibson assembly. To generate plasmids expressing mScarlet and
624 either nourseothricin resistance (pJP102) or hygromycin resistance (pJP103), an identical
625 strategy to that used in constructing pJP72 was used, except either a synthesized codon-
626 optimized nourseothricin acetyltransferase gene (sJP3) based on the sequence of
627 pUC18T-mini-Tn7T-nat (*37*) or a synthesized codon-optimized hygromycin B
628 phosphotransferase gene (sJP4) based on the sequence of *Dictyostelium* vector pDM358
629 (*36*) was used.
630
631 To generate a plasmid encoding coYki and Hygromycin resistance for rescue of *coYki -/-*
632 phenotypes (pJP119), a DNA fragment encoding coYki and a c-terminal OLLAS epitope
633 tag (*38*) was generated by PCR from a synthesized a gene encoding the coYki protein
634 (sJP5) using primers oJP101 and oJP102. To limit recombination of the transgene with
635 the endogenous coYki loci, we recoded the coYki reading frame using synonymous codon
636 replacement, resulting in a coYki gene with 73 percent nucleotide similarity to the WT
637 coYki gene but encoding an identical polypeptide. This PCR product was then cloned into
638 a KpnI and AflII digest of pJP103 using Gibson assembly.
639
640 To generate a plasmid encoding a Lifeact-mScarlet fusion protein and hygromycin
641 resistance (pJP118), a DNA fragment optimized for expression in *Capsaspora* encoding
642 the Lifeact peptide (*24*) (sJP6) was synthesized and cloned into the KpnI site of pJP103

643 by Gibson assembly. To generate a plasmid expressing Venus and Geneticin resistance
644 (pJP114), the Venus reading frame was amplified from $p_{EF1\alpha}$ -CoH2B:Venus (Addgene
645 #111877, (*12*)) using primers oJP103 and oJP104 and cloned into a KpnI and AflII digest
646 of pJP72 by Gibson assembly.
647
648 <u>*Capsaspora* Transfection</u>
649 24-well plates were prepared for transfection by inserting one sterile 12mm circular glass
650 coverslip in each well to aid in cell adhesion during transfection. *Capsaspora* cells at
651 exponential growth phase were collected by pipetting medium over attached cells,
652 resuspended to 7.5 x 10^5 cells/ml in growth medium, and then 800 µl of this cell culture
653 was added per well to the prepared 24-well plate. Cells were incubated at 23°C overnight.
654 The following day growth medium was removed from cells and was replaced by 800 µl of
655 transfection medium (Scheider's Drosophila Medium (ThermoFisher 21720024) with 10%
656 FBS (Thermofisher 26140079) supplemented with 25 µg/mL Ampicillin). After a 10-minute
657 incubation at room temperature, transfection medium was removed from the cells and
658 replaced with 500 of fresh transfection medium. Transfection mixes were then prepared:
659 100 µl of Opti-MEM I Reduced Serum Medium (ThermoFisher) was added to a 1.5ml
660 tube, and 1 µg of transfecting DNA was added to this medium (for multiple plasmids, an
661 equivalent amount of each plasmid by mass was used). 3 µl of *Trans*IT-X2® transfection
662 reagent (Mirus Bio) was then added to the tube, and the solution was immediately mixed
663 by pipetting up and down. Transfection mixes were incubated at room temperature for 5
664 minutes, and then 70 µl of the transfection mix was added dropwise to one well in the 24-
665 well plate. Cells were incubated at 23°C for 24 hours, and then the medium was removed

666 and replaced with 800 µl of growth medium. To image fluorescent transient transfectants,
667 cells were then resuspended by pipetting up and down, and 300 µl of resuspended cells
668 in growth medium were transferred to a well of an 8-well chambered coverglass slide
669 (Nunc). Cells were then imaged 48 hours after addition of growth medium using a Zeiss
670 LSM 880 confocal microscope.
671
672 Stable expression of transgenes in clonal *Capsaspora* cell lines
673 Transforming plasmids were linearized by digestion with either ScaI-HF® or AseI
674 restriction enzymes (NEB), which cut within the ampicillin resistance gene, and then
675 purified from solution and resuspended in nuclease-free water. *Capsaspora* cells were
676 transfected with the linearized plasmids using the *Trans*IT-X2® transfection reagent as
677 described above. Two days after growth medium was added to cells following
678 transfection, the growth medium was removed and replaced with 800 µl of growth medium
679 supplemented with selective drugs. Due to observations of variability in cell viability
680 between transfections, three drug concentrations were tested in parallel for each
681 transfection: for Geneticin (ThermoFisher), cells were treated at 40, 60, or 80 µg/ml; for
682 Nourseothricin (GoldBio), cells were treated at 50, 75, or 100 µg/ml; for Hygromycin B
683 (Sigma), cells were treated at 150, 200, or 250 µg/ml. Cells were grown in selective
684 medium for 2 weeks, and medium was changed every 3 days. Following selection, clonal
685 cell populations were generated by resuspending cells in growth medium by pipetting,
686 diluting cells to 3 cells/mL in growth medium, and adding 100 µl of this dilution to 200 µl
687 of growth medium per in a well in a 48-well plate (this procedure generated approximately
688 10 wells with cell growth for each 48-well plate). To image fluorescence in stably

689 transfected lines, clonal cell populations were transferred into wells in a 4-well glass
690 bottom chamber slide (Nunc), incubated at 23°C for 24 hours, and cells were then imaged
691 using a Nikon Eclipse Ti inverted microscope with NIS-Elements acquisition software.
692
693 Disruption of the Capsaspora *coYki* gene by gene targeting
694 To disrupt *coYki,* we attempted to delete a 228 bp segment of the coYki open reading
695 frame that encodes the predicted Tead-binding domain (*9*) using a PCR-generated gene
696 targeting construct. We designed a pair of primers that amplify the drug resistance
697 markers described above, including the actin (CAOG_06018) promoter and terminator,
698 with 90 bp of homology adjacent to the sequence targeted for deletion at the 5' end of the
699 primers (oJP105 and oJP106). These primers were used to amplify the Geneticin
700 resistance cassette from pJP72 by PCR, the resulting PCR product was gel purified and
701 resuspended in nuclease-free water, and WT *Capsaspora* cells were transfected with this
702 DNA as described above. Clonal populations of drug-resistant transformants were
703 generated as described above, each clone was grown to confluency in one well in a 24-
704 well plate, cells were collected by pipetting up and down, and genomic DNA was prepared
705 following the protocol described below. To genotype potential mutants, we performed
706 diagnostic PCRs on genomic DNA: to test for presence of the WT allele, we used a
707 forward primer with homology to the genome 5' of the *coYki* sequence targeted for
708 deletion (oJP107) and a reverse primer with homology within the sequence targeted for
709 deletion (oJP108). To detect successful deletion, we used oJP107 as a forward primer
710 and a reverse primer with homology to the geneticin resistance gene (oJP109). 40
711 percent of analyzed clones (6 of 15 tested clones) showed a PCR product indicative of

712 disruption of the *coYki* allele (fig. S2B). However, all clones showed a band indicative of
713 an intact WT *coYki* gene. We therefore reasoned that, at least for the culture conditions
714 used during transfection, *Capsaspora* cells may be diploid.
715
716 After the isolation of clonal lines that were heterozygous for *coYki* disruption with the
717 Geneticin resistance marker as indicated by diagnostic PCR, we attempted to disrupt the
718 remaining *coYki* allele using nourseothricin resistance as a marker. pJP102 was used as
719 a template for PCR using primers oJP105 and oJP106 to generate a nourseothricin
720 resistance cassette flanked by homology arms targeting *coYki* for disruption. This
721 construct was used to transfect a Geneticin-resistant heterozygous coYki disruption
722 mutant, and drug selection of transfectants was done as described above using
723 simultaneous selection with 60 µg/ml Geneticin and 75 µg/ml nourseothricin. After
724 generating clonal populations of drug-resistant transformants, diagnostic PCR was done
725 to detect the intact *coYki* allele as described above or a deletion allele containing the
726 nourseothricin resistance gene using primers oJP107 and oJP110. Two cell lines that
727 showed absence of the WT *coYki* allele and presence of both disruption alleles encoding
728 either Geneticin or nourseothricin resistance were used for subsequent phenotypic
729 studies.
730
731 To quantify *coYki* gene expression in a putative homozygous *coYki* disruption mutant
732 (*coYki-/-*) by qPCR, 5 x 10^6 WT or *coYki-/-* cells were collected from culture flasks while
733 in growth medium by pipetting up and down, and RNA was isolated using a RNeasy Mini
734 Plus kit (Qiagen). cDNA was made using the iScript cDNA Synthesis Kit (BioRad), qPCR

735 reactions were made using iQ™ SRBR® Green Supermix (BioRad), and qPCR was
736 performed using a CFX96 Touch Real-time PCR detection system (BioRad) with the
737 following primers: oJP111 and oJP112 to detect GAPDH, oJP113 and oJP114 to detect
738 a region of coYki within the sequence targeted for deletion, and oJP115 and oJP116 to
739 detect a region coYki 3' of the sequence targeted for deletion.
740
741 Preparing *Capsaspora* genomic DNA
742 Capsaspora genomic DNA was prepared for PCR analysis following a procedure
743 previously developed for *Dictyostelium discoideum* (*39*). Cells grown in a 24-well or 48-
744 well plate in growth medium were collected by pipetting up and down, pipetted into a 1.5
745 mL tube, centrifuged at 4000 x g for 5 minutes, and resuspended in 20 µl of nuclease-
746 free water. 20 µl of Lysis buffer (50 mM KCl, 10 mM TRIS pH 8.3, 2.5 mM $MgCl_2$, 0.45%
747 NP40, 0.45% Tween 20, and 800 µg/ml Proteinase K added fresh from a 20 mg/ml stock)
748 was added to cells, which were then incubated at room temperature for 5 minutes. Tubes
749 were then placed at 95°C for 5 minutes. After cooling to room temperature, 1 µl of this
750 sample was then used as a template in a 20-µl diagnostic PCR.
751
752 Quantification of aggregate size and circularity
753 ImageJ was used to quantify aggregate size and circularity using aggregate images.
754 Images were converted to 8-bit format, processed twice using the "Smooth" function, and
755 a Threshold was adjusted for each individual image. The Analyze Particles command was
756 then run with a gate for particle size at 400-infinity micron^2 and the "exclude on edges"
757 option selected. The returned values for aggregate area and circularity were then used

758 for further analysis. Values corresponding to more than one adjacent aggregate
759 interpreted by the algorithm as a single particle were discarded.
760
761 Assaying cell-cell adhesion and cell-substrate adhesion
762 To examine cell-cell adhesion, cells were collected from a culture flask by pipetting growth
763 media over the culture surface, diluted to 1 x 10^6 cells/mL in growth medium, and vortexed
764 to disrupt cell clumps. 1 mL volumes of cell culture were then transferred to 1.5 mL tubes
765 and incubated on a Labquake™ rotator (Thermo) for one hour at room temperature.
766 Cultures were then examined by hemocytometer, and the number of cells in each clump
767 of cells was counted for at least 35 cell clumps for each independent experiment.
768
769 To examine cell-substrate adhesion, cells were diluted to 5 x 10^5 cells/mL in growth
770 medium, and 3 mL volumes of culture were transferred per well to 6-well tissue culture-
771 treated polystyrene plates (Sigma CLS3506) and incubated at 23°C for 48 hours. For
772 agitation, plates were then placed on an orbital shaker and shaken at 140 RPM for 10
773 minutes, and then the medium from each well ("disassociated fraction") was transferred
774 to a separate tube and 3 mL of new growth medium was added to each well. 3 µL of 500
775 mM EDTA was then added to each well to detach cells from the culture surface, medium
776 was pipetted up and down over the culture surface 20 times, and this resuspension
777 ("adherent fraction") was transferred to a separate tube. Cell densities of the collected
778 fractions were determined by hemocytometer counts, total cell amounts were calculated
779 by adding the cell numbers for disassociated and adherent fractions for each condition,
780 and the percent of adherent cells for each condition was then calculated. As a control to

781 examine cell-substrate adhesion in the absence of agitation, the above protocol was
782 followed, except the orbital shaker agitation step was omitted.
783
784 Time-lapse Microscopy
785 To image cells by time-lapse transmitted light or fluorescence microscopy, cells were
786 resuspended to 1 x 10^8 cells/ml in growth medium, and 10 µl of this cell suspension was
787 added as a spot in the center of a well in a 4-well chambered coverglass slide (Nunc).
788 After a 1 hour incubation at room temperature to allow the cells to settle, the 10 µl volume
789 of medium was removed, and 1 ml of growth medium was added to the well, resulting in
790 a spot of cells in the center of the well. Cells were incubated at room temperature for 24
791 hours, a field of view with well-spaced cells was located, and then cells were imaged by
792 time-lapse microscopy using a Nikon Eclipse Ti inverted microscope with NIS-Elements
793 acquisition software. To image the effect of blebbistatin on individual cells, similar imaging
794 of cells was done, except that cells were treated with either DMSO or 1 µm bebbistatin
795 (Sigma B0560) for one hour before imaging. To image aggregates by time-lapse
796 microscopy, aggregates were generated in ultra-low attachment plates as described
797 above. During aggregate formation, 4-well chambered coverglass slides (Nunc) were
798 coated with UltraPure agarose (ThermoFisher) by making a 1% agarose in nuclease-free
799 water mixture, microwaving to dissolve the agarose, adding 800 µl of molten agarose per
800 well, and removing the molten agarose after 10 seconds by aspiration. Coated wells were
801 then allowed to dry at room temperature in a cell culture hood, resulting in a thin coating
802 of agarose. This coating functions to prevent aggregate adhesion to the glass surface.
803 After aggregate formation, aggregates were resuspended in the well by gentle pipetting,

804 and then an 800 µl volume of resuspended aggregates was transferred into one agarose-
805 coated well in a 4-well chambered coverglass slide. Aggregates were then imaged using
806 a Zeiss LSM 880 confocal microscope.
807
808 RNA-seq
809 To perform RNA-seq on *Capsaspora* cells, WT or *coYki -/-* cells were collected from
810 growth flasks by removing growth medium, adding fresh growth medium, and
811 resuspending cells attached to the flask by pipetting the medium over the surface. Cells
812 were then diluted to 2 x 10^5 cells/mL, and for each genotype two 75 cm^2 culture flasks
813 were prepared by adding 16 mL of culture dilution to each flask. Culture flasks were
814 incubated at 23°C for 2 days, and then cells were collected by pipetting growth medium
815 over attached cells. Cells were collected by centrifugation at 2100 x g for 5 minutes, and
816 then all cells for each genotype were combined, resuspended in 500 µl of growth medium,
817 and transferred to a microcentrifuge tube. RNA was then prepared with the RNEasy Plus
818 Mini Kit (Qiagen) using the QIAshredder spin column (Qiagen) to homogenize the lysate.
819 RNA samples were run on an Agilent Tapestation 4200 to determine level of degradation,
820 thus ensuring only high quality RNA was used (RIN Score 8 or higher). A Qubit® 4.0
821 Fluorimeter (ThermoFisher) was used to determine the concentration prior to staring
822 library prep. One microgram of total DNAse-treated RNA was then prepared with the
823 TruSeq Stranded mRNA Library Prep Kit (Illumina). Poly-A RNA was purified and
824 fragmented before strand specific cDNA synthesis. cDNA was then A-tailed and indexed
825 adapters were ligated. After adapter ligation, samples were PCR-amplified and purified
826 with AmpureXP beads, then validated again on the Agilent Tapestation 4200. Before

827 being normalized and pooled, samples were quantified by Qubit then run on an Illumina
828 NextSeq 500 using V2.5 reagents. Three biological replicates were sequenced for each
829 genotype, with 22-31 million reads generated per sample. The fastq files were checked
830 for quality using fastqc (v0.11.2)(*40*) and fastq_screen (v0.4.4)(*41*). Fastq files were
831 mapped to GCF_000151315.2 reference assembly using STAR (*42*). Read counts were
832 then generated using featureCounts (*43*). Trimmed Mean of M-values normalization and
833 differential expression analysis were performed using edgeR (*44*) (false discovery rate
834 (FDR) <=0.05, absolute log2(fold change) >= 0.5, log(counts per million) >=0).
835 Phylogenetic trees were downloaded from PhyloDB (*45*) corresponding to *Capsaspora*
836 (PhyID 101) and pairwise distances for each gene were extracted using an R package
837 ape (*46*). Closest Human and mouse orthologues were then extracted and used to
838 annotate the *Capsaspora* genes. These annotated gene names were then used with IPA
839 (*47*) (QIAGEN Inc., https://www.qiagenbioinformatics.com/products/ingenuity-pathway-
840 analysis) to get significantly enriched pathways in "Diseases and Bio Functions" category.
841 To identify functional enrichment in the sets of genes upregulated or downregulated in
842 *coYki -/-* cells, DAVID Functional Annotation Tool (*48*) was used to identify functional
843 categories with FDR < 0.05 using all *Capsaspora* genome genes as the gene population
844 background.
845
846 Statistics
847 All statistics were done using Prism (GraphPad software, San Diego, CA). Student's t-
848 test was done to compare differences between two groups, and one-way analysis of

849 variance (ANOVA) with a post-hoc test was used to compare differences among groups
850 greater than two.
851
852 Gene nomenclature
853 In the manuscript we use italicized text to refer to a gene (e.g., *coYki)*, unitalicized text
854 to refer to a protein (e.g., coYki), "-/-" to indicate a homozygous deletion mutant (e.g.,
855 *coYki -/-),* and ">" to indicate a promoter driving the expression of a gene (e.g., *EF1 >*
856 *coYki).*

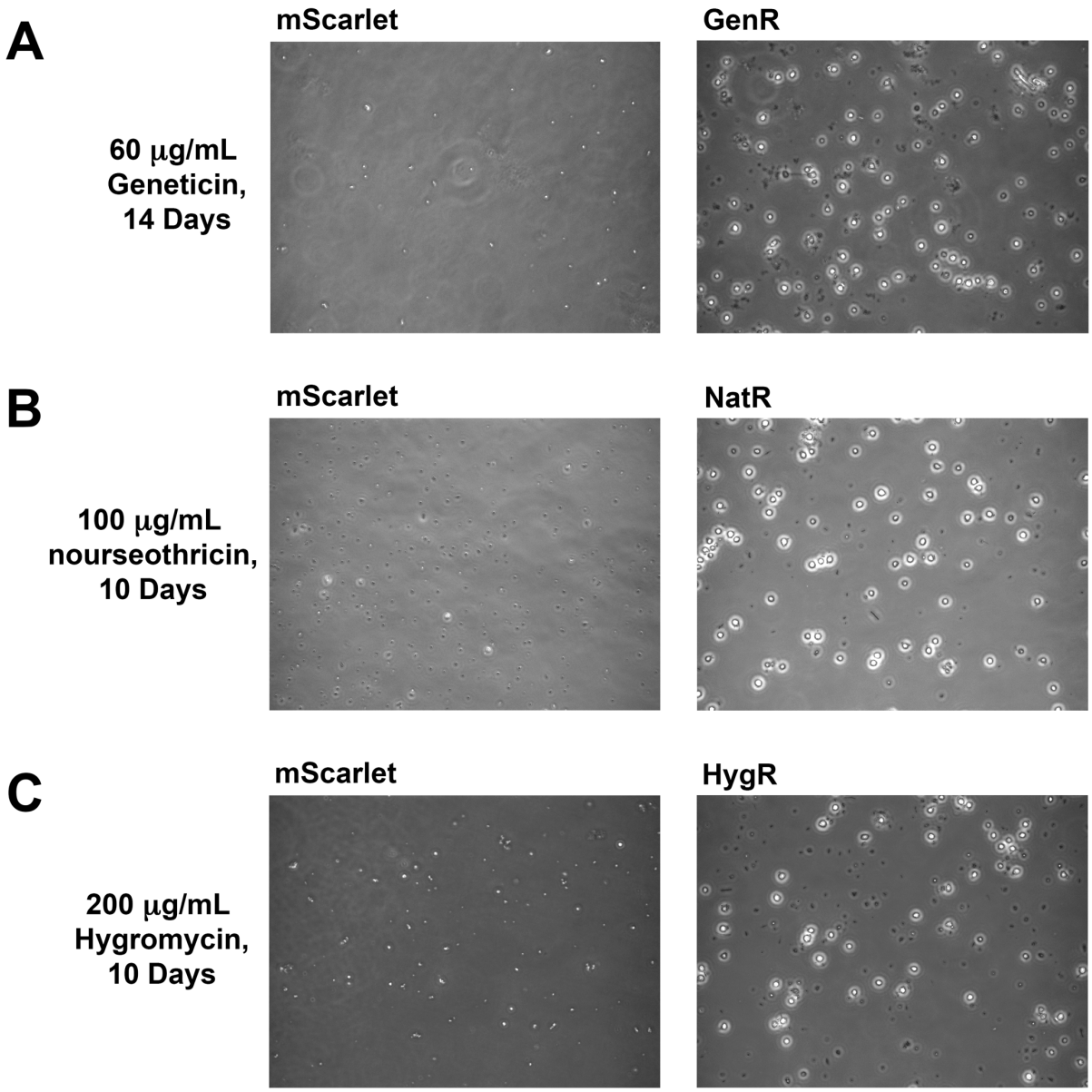

857

858 **Fig. S1. Transfection of *Capsaspora* with genes encoding antibiotic resistance**
859 **markers results in viable cell populations after drug treatment.** Cells were
860 transfected with plasmids encoding mScarlet with no antibiotic marker (pJP71), GenR
861 (pJP72), NatR (pJP102), or HygR (pJP103) genes and were treated with the indicated
862 antibiotics 2 days after transfection for the indicated time period. Representative images

863 of the population are shown. Round, phase-bright cells are visible in populations
864 transfected with resistance markers but not cells transfected with mScarlet.
865
866
867

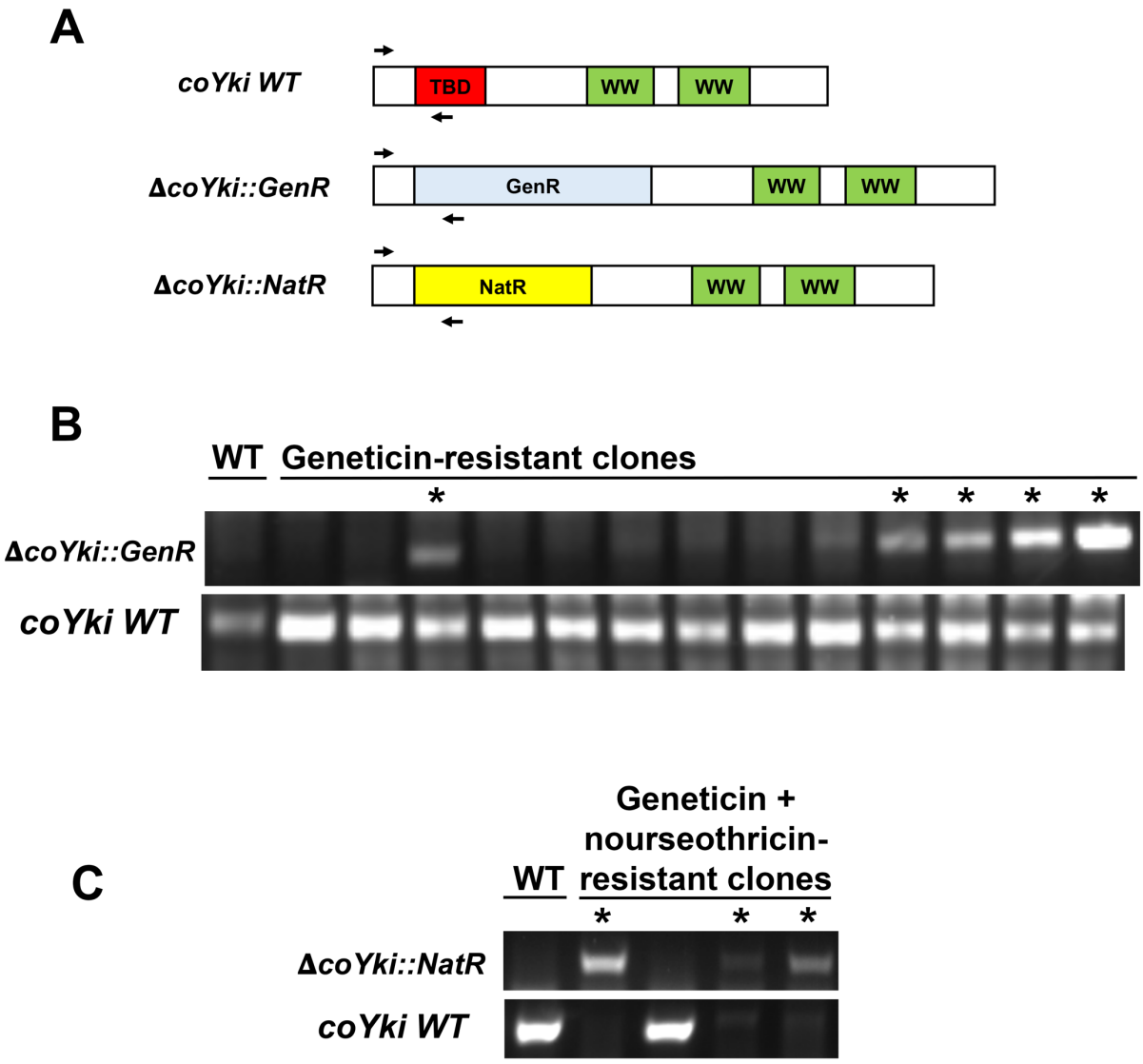

868

869

870 **Fig. S2. Diagnostic PCR of putative coYki deletion clonal cell lines. (A)** Diagram of
871 primer pairs used to evaluate the presence of the WT *coYki* allele (*coYki* WT), a deletion
872 of a region of *coYki* using the GenR marker (Δ*coYki::GenR*), or a deletion of a region of
873 coYki using the NatR marker (Δ*coYki::NatR*). TBD, Tead-binding domain; WW, WW
874 domain; GenR, Geneticin resistance; NatR, nourseothricin resistance. **(B)** WT cells were
875 transfected with a gene-targeting construct encoding GenR designed to delete the TBD

876 in the *coYki* gene by homologous recombination (see figure 1G in main text). Following
877 transfection and drug selection, clonal populations of transfectants were generated and
878 analyzed by diagnostic PCR using the indicated primer pairs. "*" indicates a clone
879 showing a PCR product indicative of heterozygous coYki disruption. **(C)** A clonal cell line
880 with a diagnostic PCR result indicating the disruption of a coYki allele with GenR was
881 transfected with a gene-targeting construct encoding NatR designed to delete the TBD in
882 the *coYki* gene. After selection with both Geneticin and nourseothricin, clonal populations
883 of transfectants were generated and analyzed by diagnostic PCR using the indicated
884 primer pairs. "*" indicates a clone showing a PCR product indicative of homozygous coYki
885 disruption.
886
887

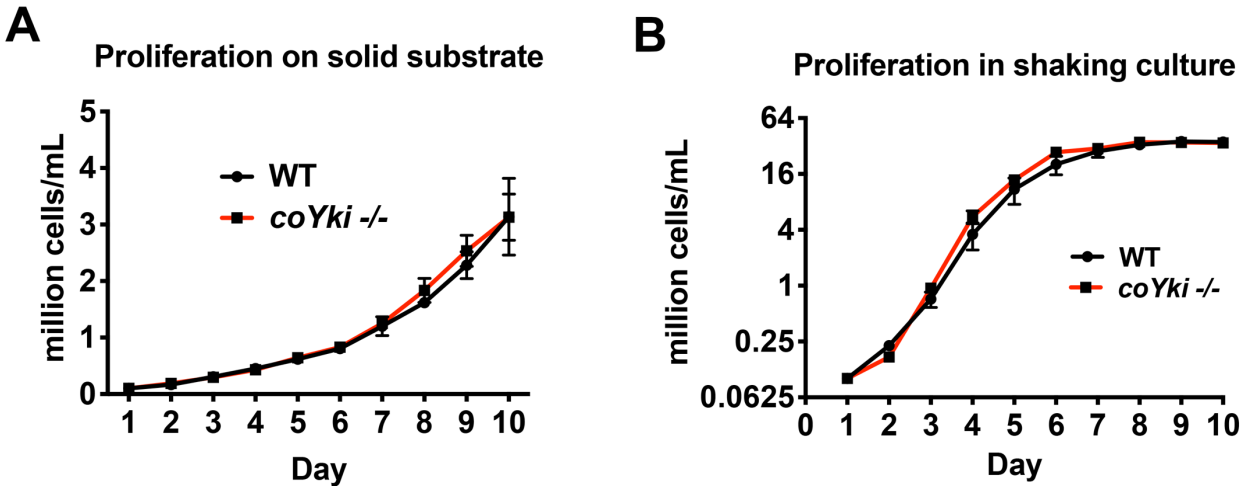

Fig. S3. WT and *coYki -/-* cells proliferate at a similar rate. (A) To examine proliferation on a solid substrate, cells were grown in wells in a 24-well plate, and each day cells within one well were resuspended and counted. **(B)** To examine proliferation in shaking culture, cells were grown in flasks on an orbital shaker, and an aliquot of cells was collected and counted daily. Values are mean ± SEM ($n \geq 3$). Absence of error bars indicates that error is smaller than the plot symbol.

898

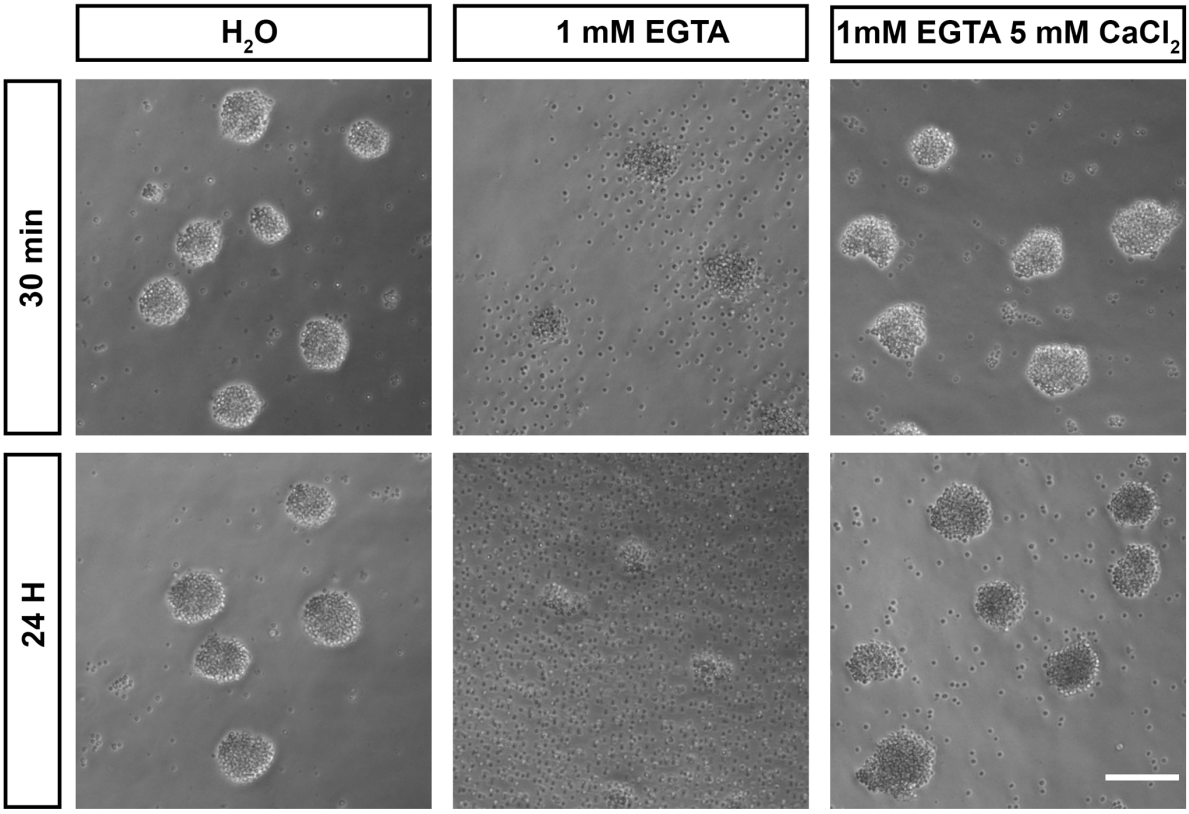

899

900 **Fig. S4. Calcium is required for adhesion in *Capsapsora* cell aggregates.**
901 *Capsaspora* aggregates were treated with water (vehicle control), the calcium chelator
902 EGTA, or EGTA with an excess of calcium. At 30 minutes aggregates treated with EGTA
903 had begun to disassociate, with further disassociation evident at 24 hours. Simultaneous
904 addition of an excess of calcium blocked this disassociation.

905

906

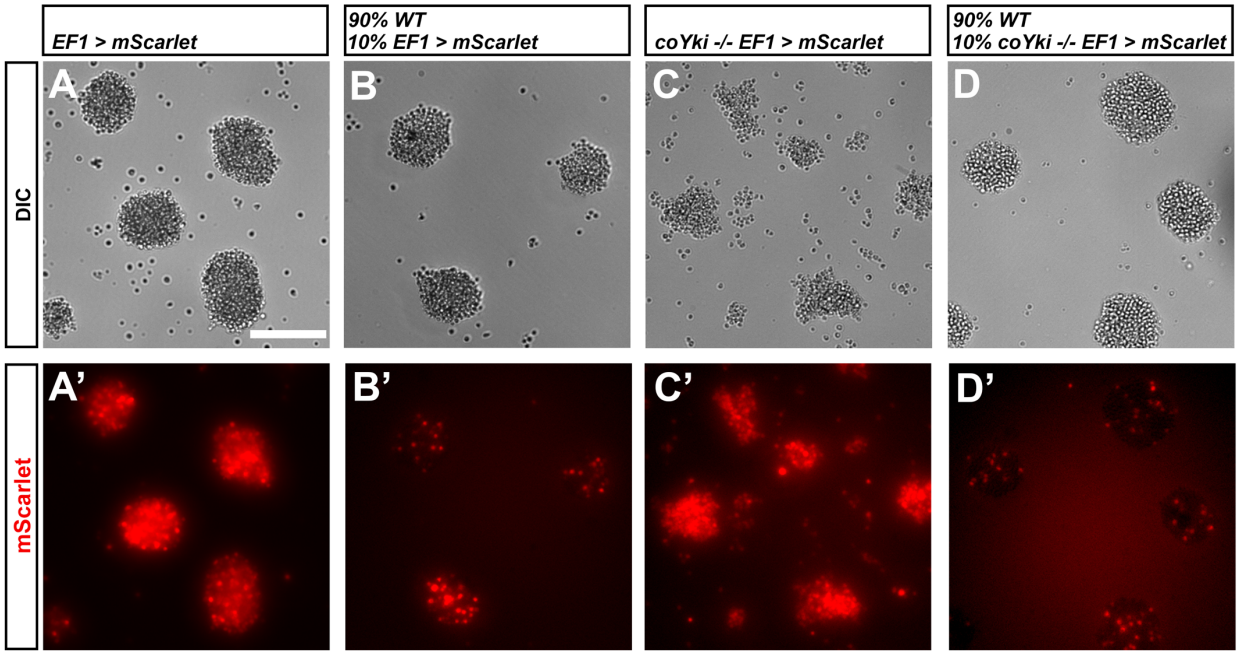

Fig. S5. *coYki -/-* cells adhere to and integrate within WT aggregates like WT cells. **(A-D)** Cells expressing mScarlet in the WT background **(A-B)** or in the *coYki -/-* mutant background **(C-D)** were allowed to aggregate as a homogeneous population **(A, C)** or were mixed with 90% WT cells and allowed to aggregate **(B, D)**. Individual mScarlet-labeled *coYki -/-* cells associate with WT cells within aggregates **(D')** in an organization like that of cells from the WT background labeled with mScarlet **(B')**. Scale bar is 75 microns.

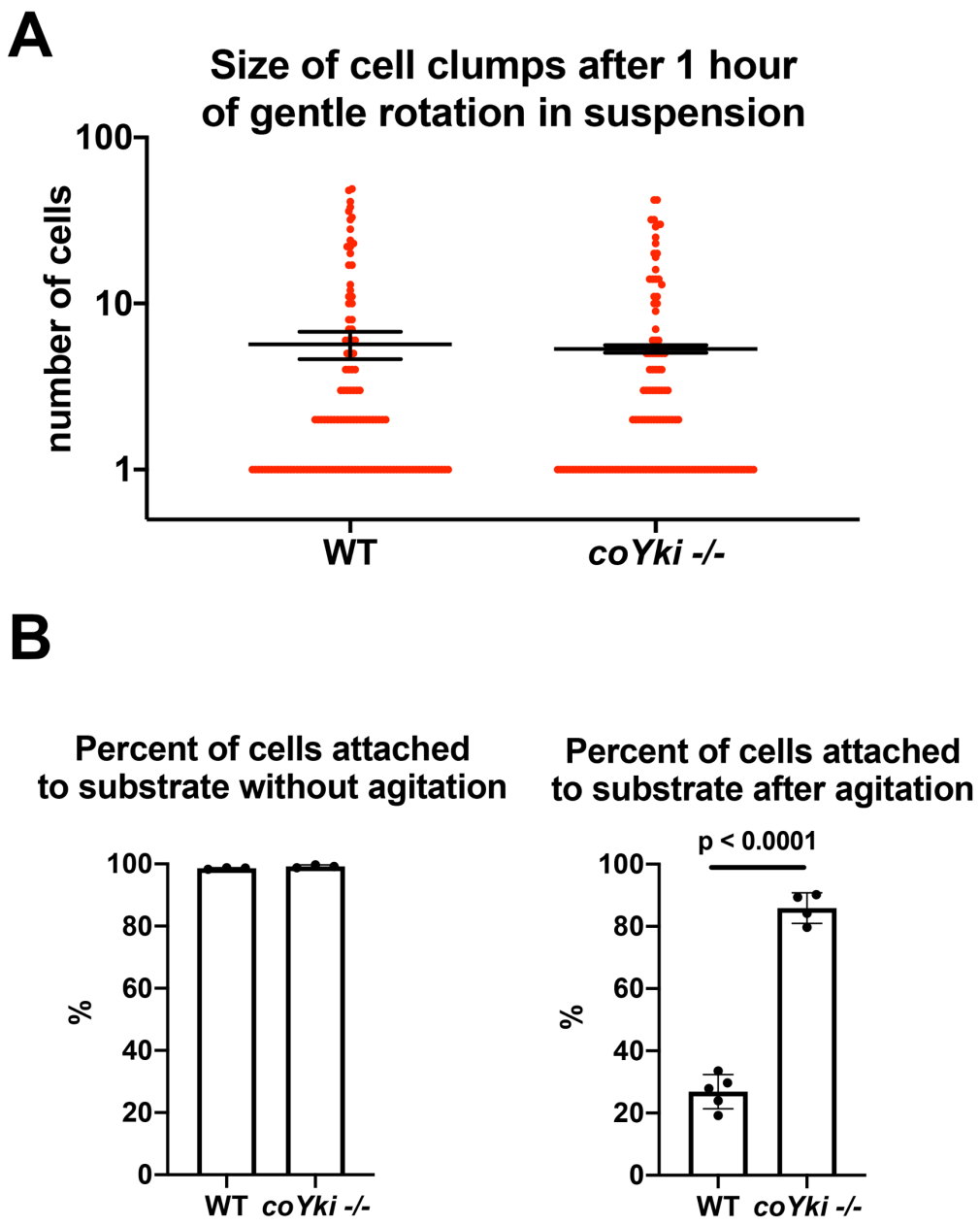

Fig. S6. coYki affects cell-substrate adhesion but shows no effect on cell-cell adhesion. (A) To examine cell-cell adhesion, cells in suspension were gently rotated for an hour to stimulate clump formation through cell-cell adhesion. Cultures were then examined by hemocytometer and the number of cells per clump was counted. Each red circle indicates the number of cells in a single clump, and error bars indicate the mean ± SEM of the average number of cells per clump from 3 independent experiments. Absence

925 of error bars indicates that error is smaller than the plot symbol. The difference in average
926 number of cells per clump between WT and *coYki -/-* is not significant (t-test). **(B)** To
927 examine cell-substrate adhesion, adherent cell cultures were either agitated on a rotary
928 shaker for 10 minutes or left untreated, and then the number of adhered and unadhered
929 cells in each culture was counted and the percent of cells adhered to the culture substrate
930 was calculated. The difference between WT and *coYki -/-* is significant for the percent of
931 cells attached to substrate after agitation ($p < 0.0001$, t-test).

932 **Movie S1. Aggregation of WT or *coYki -/-* cells over 6 days on a low-adherence**
933 **surface.** Time units are given in days.
934
935 **Movie S2. WT and *coYki -/-* cells on a glass surface.**
936
937 **Movie S3. *coYki -/-* cells expressing a *coYki* rescue transgene.**
938
939 **Movie S4. Basal region of *Capsaspora* cells expressing Lifeact-mScarlet.**
940
941 **Movie S5. Medial region of WT or *coYki -/-* cells expressing Lifeact-mScarlet.**
942
943 **Movie S6. Actin dynamics in a single *coYki -/-* cell expressing Lifeact-mScarlet.**
944
945 **Movie S7. WT or *coYki -/-* cells expressing Lifeact-mScarlet within an aggregate.**
946
947 **Movie S8. Treatment of *coYki -/-* cells expressing Lifeact-mScarlet with blebbistatin**
948 **reduces blebbing.**
949
950

951 **Data S1. Sequences of synthesized gene fragments used in this study**

952

953 **Data S2. Sequences of oligonucleotides used in this study**

954

955 **Data S3. Plasmids constructed for this study**